THE JOURNAL OF BIOLOGICAL CHEMISTRY VOL. 284, NO. 48, pp. 33369–33376, November 27, 2009

Apolipoprotein A-V N-terminal Domain Lipid Interaction Properties *in Vitro* Explain the Hypertriglyceridemic Phenotype Associated with Natural Truncation Mutants*

Received for publication, July 3, 2009, and in revised form, October 6, 2009 Published, JBC Papers in Press, October 13, 2009, DOI 10.1074/jbc.M109.040972

Kasuen Wong-Mauldin[‡§1], **Vincent Raussens**[¶2], **Trudy M. Forte**[‡], **and Robert O. Ryan**[‡§3]

From the [‡]*Center for Prevention of Obesity, Diabetes and Cardiovascular Disease, Children's Hospital Oakland Research Institute, Oakland, California 94609, the* [§]*Department of Nutritional Sciences and Toxicology, University of California, Berkeley, California 94720, and the* [¶]*Center for Structural Biology and Bioinformatics, Laboratory for Structure and Function of Biological Membranes, Faculté des Sciences, Université Libre de Bruxelles, CP 206/2, B-1050 Brussels, Belgium*

The N-terminal 146 residues of apolipoprotein (apo) A-V adopt a helix bundle conformation in the absence of lipid. Because similarly sized truncation mutants in human subjects correlate with severe hypertriglyceridemia, the lipid binding properties of apoA-V(1–146) were studied. Upon incubation with phospholipid *in vitro*, apoA-V(1–146) forms reconstituted high density lipoproteins 15–17 nm in diameter. Far UV circular dichroism spectroscopy analyses of lipid-bound apoA-V(1–146) yielded an α-helix secondary structure content of 60%. Fourier transformed infrared spectroscopy analysis revealed that apoA-V(1–146) α-helix segments align perpendicular with respect to particle phospholipid fatty acyl chains. Fluorescence spectroscopy of single Trp variant apoA-V(1–146) indicates that lipid interaction is accompanied by a conformational change. The data are consistent with a model wherein apoA-V(1–146) α-helices circumscribe the perimeter of a disk-shaped bilayer. The ability of apoA-V(1–146) to solubilize dimyristoylphosphatidylcholine vesicles at a rate faster than full-length apoA-V suggests that N- and C-terminal interactions in the full-length protein modulate its lipid binding properties. Preferential association of apoA-V(1–146) with murine plasma HDL, but not with VLDL, suggests that particle size is a determinant of its lipoprotein binding specificity. It may be concluded that defective lipoprotein binding of truncated apoA-V contributes to the hypertriglyceridemia phenotype associated with truncation mutations in human subjects.

The helix bundle motif is a common molecular architecture in proteins (1). Exchangeable apolipoproteins (apo)[4] are known to adopt this conformation, which supports their dual existence in alternate lipid-free and lipid-bound states. Classic examples of the helix bundle structure include the N-terminal (NT) domains of apoE (2) and apoA-I (3) as well as apolipophorin III (4). In the case of apoE and apoA-I, the helix bundle motifs are present within the context of a larger protein structure. In each of these examples the bundle exists as an up-and-down series of amphipathic α-helices wherein the hydrophobic face of each helical segment orients toward the interior of the bundle. At the same time, the polar face of the amphipathic helices is directed toward the exterior of the bundle. In this way the globular structure is stabilized by hydrophobic helix-helix interactions and is conferred with water solubility through projection of polar and charged amino acid side chains toward the aqueous milieu. Upon interaction with lipid surfaces, the helix bundle is postulated to unfurl, adopting an extended open conformation that promotes interaction between the hydrophobic faces of amphipathic helices and the lipid surface. Essentially, lipid binding of helix bundle apolipoproteins substitutes helix-helix contacts in the bundle for helix-lipid contacts that stabilize the lipid-bound state.

In 2001 a new apolipoprotein, termed apoA-V, was reported that profoundly affects plasma TG levels (5, 6). Structural studies revealed that apoA-V is a two-domain protein (7) and that its N-terminal 146 residues adopt a helix bundle structure in the absence of lipid (8). Truncated apoA-V proteins in this size range have been reported in human subjects with severe hypertriglyceridemia (HTG) (9, 10). One of these truncation mutants, Q139X apoA-V, does not associate with VLDL or HDL in circulation (9). By contrast, full-length apoA-V is found on both of these lipoprotein classes in normolipidemic subjects (11). Insofar as these individuals had no other common mutations known to cause HTG, it is likely that a lipid-binding defect in truncated apoA-V is associated with the HTG phenotype. To address this mechanistically, the lipid interaction properties of recombinant apoA-V(1–146) were investigated. The results obtained provide a molecular explanation for the correlation between naturally occurring C-terminal (CT) truncations in apoA-V and HTG.

EXPERIMENTAL PROCEDURES

Site-directed Mutagenesis and Recombinant Protein Expression—Recombinant human apoA-V and CT truncation variants were produced in *Escherichia coli* and isolated as

* This work was supported, in whole or in part, by National Institutes of Health Grant HL-073061.

[1] Recipient of a Gates Millennium Scholarship.

[2] Senior Research Associate for the National Fund for Scientific Research (Belgium).

[3] To whom correspondence should be addressed: CHORI, 5700 Martin Luther King Jr. Way, Oakland, CA 94609. Tel.: 510-450-7645; Fax: 510-450-7910; E-mail: rryan@chori.org.

[4] The abbreviations used are: apo, apolipoprotein; HTG, hypertriglyceridemia; DMPC, dimyristoylphosphatidylcholine; NT, N terminus; CT, C terminus; HDL, high density lipid; ATR-FTIR, attenuated total reflectance Fourier transformed infrared spectroscopy; VLDL, very low density lipid; PL-C, phospholipase C; Tricine, *N*-[2-hydroxy-1,1-bis(hydroxymethyl)ethyl]glycine; TG, triacylglycerol.

described (12). ApoE3 NT was prepared as described by Fisher *et al.* (13). Recombinant apoA-I was prepared as described by Ryan *et al.* (14). Site-directed mutagenesis was performed with the QuikChange II XL site-directed mutagenesis kit (Stratagene). Primers were designed to introduce a premature stop codon or to substitute Trp^{5} with Phe, substituteTrp^{97} with Phe, or substitute Asn^{45}, Leu^{73}, Val^{117}, or Leu^{128} of Trp-null apoA-V(1–146) with Trp. In all cases, introduction of the desired mutations was verified by DNA sequencing.

Interaction of ApoA-V(1–146) with Phospholipid—Dimyristoylphosphatidylcholine (DMPC) bilayer vesicles were incubated with apoA-V(1–146) at a ratio of 5:1 by weight as previously described (12). The size distribution of DMPC-apoA-V(1–146) complexes was evaluated by nondenaturing gradient PAGE as described by Nichols *et al.* (15).

Circular Dichroism Spectroscopy—CD spectroscopy measurements were performed on an AVIV 410 spectrophotometer. Far UV CD scans were obtained between 195 and 250 nm in 10 mM sodium phosphate, pH 7.4, using a protein concentration of 0.5 mg/ml determined from the absorbance at 280 nm. The α-helical content was calculated with the self-consistent method using Dicroprot version 2.6 (16).

Infrared Spectroscopy—Attenuated total reflectance Fourier transformed infrared spectroscopy (ATR-FTIR) spectra were recorded on a Bruker IFS 55 infrared spectrophotometer equipped with a reflectance accessory and a polarizer mount assembly with an aluminum wire grid on a KRS-5 element. The internal reflection element was a germanium ATR plate (50 mm × 20 mm × 2 mm) with an aperture angle of 45° yielding 25 internal reflections. Oriented multilayers were formed by slow evaporation of ~10 μl of apoA-V(1–146)·DMPC (1 mg/ml) on one side of the ATR plate under a gentle stream of nitrogen, yielding a semi-dry film bearing residual water molecules. The ATR plate was then sealed in a universal sample holder. The spectra were recorded at a 2 cm^{-1} nominal resolution. A total of 128 accumulations were performed to improve the signal/noise ratio. The spectrometer was constantly purged with dry air. All of the measurements were made at 25 °C.

Secondary structure measurements were carried out on samples following deuteration for 1 h as previously described (17). Briefly, Fourier self-deconvolution was applied to enhance the resolution of the spectra in the amide I region. Least squares iterative curve fitting was performed to fit different components of the amide I band revealed by the self-deconvolution to the nondeconvolved spectrum between 1700 and 1600 cm^{-1}. The proportion of various secondary structural elements was computed as reported in Ref. 17.

Analytical Procedures—Protein concentrations were determined with the bicinchoninic acid assay (Pierce) with bovine serum albumin as standard.

Fluorescence Spectroscopy—Fluorescence spectra were obtained on a Horiba Jobin Yvon FluoroMax-4 luminescence spectrometer. Protein (0.5 μg/μl) was dissolved in 20 mM sodium phosphate, pH 7.4, 150 mM NaCl. The samples were excited at 295 nm, and emission was collected from 300 to 450 nm (slit width, 2.0 nm). For Trp fluorescence quenching studies DMPC-bound apoA-V(1–146) samples (200 μg of protein in 400 μl of total volume) were excited at 295 nm, and emission was monitored at their λ_{max} (slit width, 2.0 nm). Quenching of Trp fluorescence in 20 mM sodium phosphate, pH 7.4, 150 mM NaCl by the addition of either KI or acrylamide in the concentration range 0.0 – 0.6 M was measured. The solution of KI contained 1 mM sodium thiosulfate to prevent formation of free iodine, and all of the readings were corrected for dilution. For acrylamide quenching, fluorescence intensities were corrected for the absorption of acrylamide at 295 nm,

$$I_{corr.} = 10^{\left(\frac{0.23[acryl]}{2}\right)} I_{meas.} \quad \text{(Eq. 1)}$$

where 0.23 is the molar extinction coefficient of acrylamide at 295 nm (18). The data were analyzed using the following Stern-Volmer equation,

$$F_0/F = 1 + K_{SV}[Q] \quad \text{(Eq. 2)}$$

where F_0 and F represent the emission intensity maximum in the absence and presence of quencher, respectively, and [Q] is quencher concentration. The collisional quenching constant (K_{SV}) was determined from the initial slope of plots of F_0/F *versus* [Q].

DMPC Vesicle Solubilization—DMPC bilayer vesicles were prepared by extrusion through a 100-nm filter as described by Weers *et al.* (19). Stock solutions of protein and lipid vesicles were prepared in 50 mM citrate, pH 3.0, 150 mM NaCl. 500 μg of DMPC was incubated in the absence or presence of 100 μg of apolipoprotein (total volume, 400 μl) at 23 °C in a thermostatted cell holder. Sample right angle light scattering intensity was monitored on a PerkinElmer Life Sciences LS50B luminescence spectrometer as a function of time, with the excitation and emission monochromaters set at 600 nm (slit width, 2 nm).

LDL Binding Assay—Human LDL (Intracel) was incubated for 90 min at 37 °C in the presence or absence of *Bacillus cereus* phospholipase C (PL-C) (0.6 unit/50 μg of LDL protein). Where indicated, apolipoprotein (50 μg/50 μg of LDL protein) was included in the reaction mixture. The incubations were conducted in 50 mM Tris-HCl, pH 7.5, 150 mM NaCl, and 2 mM $CaCl_2$ in a total sample volume of 200 μl. Sample turbidity was measured at 340 nm on a Spectramax 340 microtiter plate reader (Sunnyvale, CA) (20).

Incubation of ApoA-V(1–146) with Isolated HDL and VLDL from Apoa5$^{-/-}$ mice—Blood from male apoA-V-deficient mice (average age 4 months, fasted for 4 h) was collected into tubes containing K_3EDTA and kept on ice. After centrifugation at 2,000 × *g* for 10 min at 4 °C, the plasma was removed and treated with a protease inhibitor mixture as described by Nelbach *et al.* (21). Plasma was pooled, stored at 4 °C, and used within 2 days. Plasma VLDL and HDL were isolated by sequential ultracentrifugation as described by Lindgren *et al.* (22). Isolated VLDL ($d < 1.006$ g/ml) or HDL ($d = 1.063$–1.21 g/ml) was incubated with recombinant apoA-V(1–146) (weight ratio, 10:1, lipoprotein protein:apoA-V(1–146)) for 1 h at 22 °C in Tris-buffered saline. After incubation, ultracentrifugation was performed to reisolate VLDL (d < 1.006 g/ml, top fraction) and HDL ($d < 1.21$ g/ml, top fraction). The bottom, lipoprotein-free, fractions from each tube were also recovered. Similar studies were carried out with full-length recombinant apoA-V.

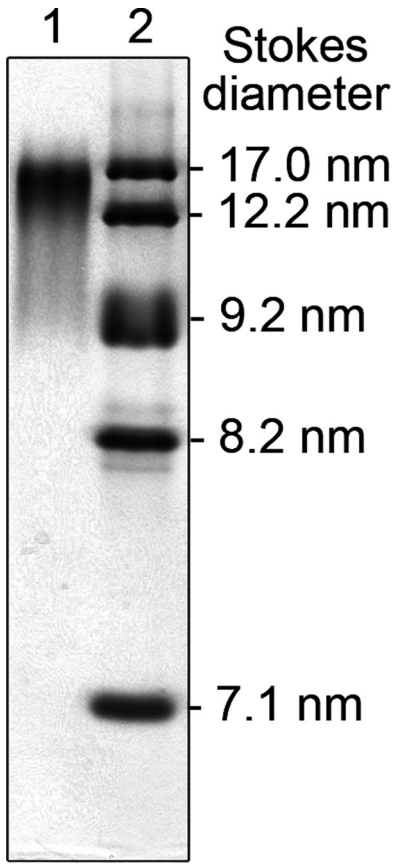

FIGURE 1. **Native gradient PAGE of apoA-V(1–146)·DMPC complexes.** ApoA-V(1–146)·DMPC complexes were prepared as described under "Experimental Procedures" and applied to a 4–20% acrylamide gradient gel. Following electrophoresis the gel was stained with Coomassie Blue. *Lane 1*, apoA-V(1–146)·DMPC complexes (5 μg of protein); *lane 2*, molecular size standards.

Immunoblotting—For immunoblotting, the protein samples were separated on a 10–20% acrylamide gradient, Tricine-SDS slab gel (Invitrogen). The proteins were electrophoretically transferred to a 0.2-μm polyvinylidene difluoride membrane (Bio-Rad) at a constant current of 150 mA for 3 h. Nonspecific binding sites on the membrane were blocked with 0.1% TTBS (0.1% Tween 20, 20 mM Tris, and 150 mM NaCl, pH 7.2) overnight, at 4 °C with rotation. Goat anti-apoA-V IgG (12) (1:10,000 dilution in 0.1% TTBS) was incubated with the membrane for 1 h with rotation. The mixture was washed three times in TTBS, and then HRP-conjugated donkey anti-goat secondary antibody was incubated with the membrane for 1 h. After washing, the membrane was incubated with SuperSignal West Femto maximum sensitivity substrate (Pierce) and exposed to CL-Xposure Film (Pierce) for less than 10 s. The film was developed using a Kodak M35A X-OMAT processor.

RESULTS

Characterization of ApoA-V(1–146) Binding to Phospholipid Vesicles—Incubation of apoA-V(1–146) with a DMPC vesicle dispersion caused a decrease in solution light scattering intensity consistent with formation of lipid complexes (*i.e.* reconstituted HDL). Native gradient PAGE analysis revealed a discrete population of particles with a Stoke's diameter in the range of 15–17 nm (Fig. 1). These complexes, which are similar in size to discoidal particles formed with full-length apoA-V (12), indicate that the NT domain of apoA-V possesses intrinsic lipid binding capability.

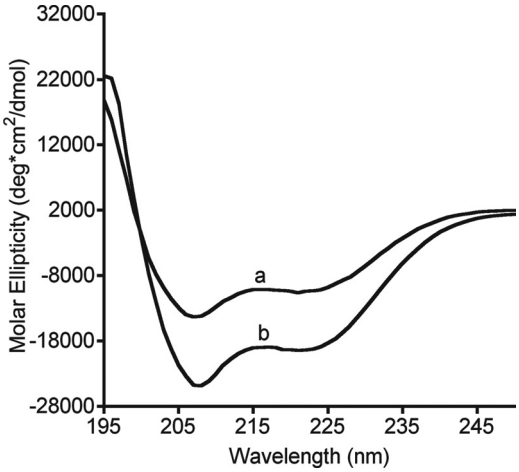

FIGURE 2. **Effect of lipid interaction in the spectroscopic properties of apoA-V(1–146).** Far UV circular dichroism spectra of lipid-free apoA-V(1–146) (*curve a*) and apoA-V(1–146)·DMPC (*curve b*) were collected in 10 mM sodium phosphate at a protein concentration of 0.5 mg/ml.

Far UV CD Spectroscopy Analysis—The effect of lipid association on the secondary structure content of apoA-V(1–146) was evaluated by far UV CD spectroscopy (Fig. 2). The spectrum of lipid-free apoA-V(1–146) (Fig. 2, *curve a*) has minima at 208 and 222 nm, indicating the presence of α-helix secondary structure. Deconvolution of the spectrum yielded a value of 40% α-helix. Upon interaction with DMPC, however, a significant enhancement in α-helix content was noted as seen by the increase in negative ellipticity at 208 and 222 nm (Fig. 2, *curve b*). Deconvolution of the spectra yielded a value of 60% α-helix structure.

Orientation of α-Helices in ApoA-V(1–146) Lipid Complexes—ATR-FTIR spectra of apoA-V(1–146)·DMPC complexes were recorded with parallel and perpendicular polarized light (Fig. 3). The amide I region of the spectra (1700–1600 cm^{-1}) was used to determine the orientation of α-helices in apoA-V(1–146) relative to DMPC hydrocarbon chains of the bilayer component of the reconstituted HDL. A dichroic spectrum was obtained by subtracting the spectrum recorded with perpendicular polarized light from the spectrum recorded with parallel polarized light. Bands corresponding to dipoles that orient parallel to the hydrocarbon chain progression observed for saturated hydrocarbon chains had a positive deviation in the dichroic spectrum. Thus, these orient parallel to the normal of the germanium plate. The apoA-V(1–146) helix orientation was determined using the amide I band. In the dichroic spectrum, a negative deviation at ~1650 cm^{-1} is observed, indicating a parallel orientation of the associated dipole to the surface of the germanium plate and, thus, a perpendicular orientation with respect to a vector normal to the face of the disk. From the secondary structure of apoA-V(1–146) and the frequency of the negative deviation, it may be concluded that the dipole responsible for this deviation is associated with α-helices, which orient in the direction of the helical axes. Thus, the negative deviation observed indicates that the helices are primarily oriented per-

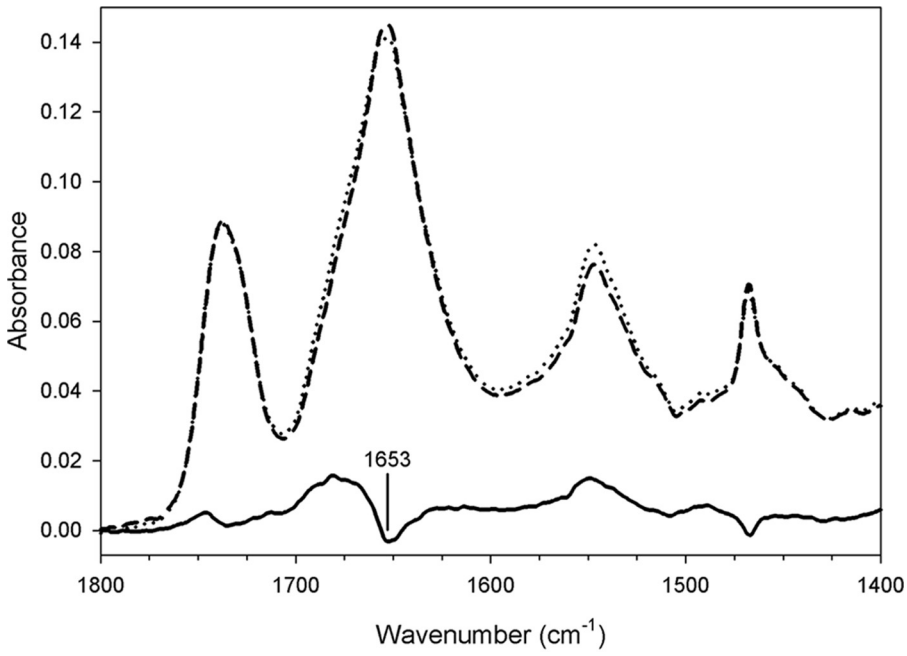

FIGURE 3. **Infrared spectroscopy analysis of apoA-V(1–146)·DMPC complexes.** ATR-FTIR spectra of apoA-V(1–146)·DMPC disks recorded with light polarized parallel to a normal to the surface of the internal reflection element (*dotted line*) and with light polarized perpendicular to the normal to the surface (*dashed line*). Both spectra have been rescaled based on the lipid band at 1740 cm^{-1}. The *solid line* represents the calculated dichroic spectrum. To improve visualization, the dichroic spectrum is shown at 2× intensity *versus* the other spectra.

TABLE 1

Fluorescence properties of apoA-V(1–146) variants

Spectra were recorded on a Jobin Yvon FluoroMax-4 luminescence spectrometer. Emission spectra were recorded from 300 to 450 nm (excitation, 295 nm) in 20 mM sodium phosphate, pH 7.4, 150 mM NaCl (slit width, 2.0 nm for the excitation and emission monochromators) at a protein concentration of 0.5 mg/ml. In DMPC-bound samples, a DMPC:protein ratio of 5:1 was used.

ApoA-V(1–146) single Trp variant	Predicted Trp location[a]	λ_{max}[b]	
		Lipid-free	DMPC-bound
		nm	
Trp^{5}	Extreme N terminus	350	345
Trp^{45}	Polar face	350	346
Trp^{73}	Nonpolar face	349	338
Trp^{97}	Linker	349	348
Trp^{117}	Nonpolar face	340	335
Trp^{128}	Nonpolar face	349	338

[a] Based on primary sequence analysis using the Coils program (23) and Edmundson helical wheel diagrams (24).

[b] λ_{max} is the wavelength of maximum fluorescence emission. The values reported are the means of at least three independent determinations. In all cases, the standard deviation was ≤1 nm.

pendicular to the normal vector of the disk and, therefore, perpendicular to the hydrocarbon chains of the lipids.

Quantification of the secondary structure conformers present was performed on samples subjected to deuteration. The predominant secondary structure conformer present is α-helix (61%), in good agreement with the value determined by CD spectroscopy.

Trp Fluorescence Emission Analysis—The wavelength of maximum fluorescence emission of tryptophan residues is a useful tool to monitor changes and to make inferences regarding local structure and environment. Single Trp apoA-V(1–146) variants were generated to explore the effect of lipid association on specific regions of apoA-V(1–146). All of the apoA-V(1–146) variants generated were characterized by far UV CD spectroscopy. No significant differences were noted, indicating that the conserved substitution mutations introduced did not alter the secondary structure content of the protein. ApoA-V possesses two naturally occurring Trp, at positions 5 and 97. Primary sequence analysis using the Coils program (23) and Edmundson helical wheel diagrams (24) indicate that these Trp are located at the extreme N terminus (Trp^{5}) and in a loop or "linker" segment between α-helices (Trp^{97}). When these Trp residues were mutated to generate the corresponding single Trp apoA-V(1–146) variants, fluorescence emission analysis revealed they are largely exposed to solvent in the absence of lipid and undergo relatively small blue shifts in their wavelength of maximum fluorescence emission upon interaction with DMPC (Table 1). To extend this approach, a panel of single Trp apoA-V(1–146) variants was constructed via site-directed mutagenesis. For these studies Asn^{45}, Leu^{73}, Val^{117}, and Leu^{128} were individually mutated to Trp in the context of a Trp-null apoA-V(1–146) background. Based on sequence analysis, Trp^{45} is predicted to reside on the polar face of an amphipathic α-helix, whereas the Trp^{73}, Trp^{117}, and Trp^{128} are postulated to reside on the hydrophobic face of amphipathic α-helices. Trp fluorescence emission spectra of these single Trp apoA-V(1–146) variants were analyzed in lipid-free and lipid-bound states (Table 1). Whereas Trp^{45} apoA-V(1–146) undergoes a 4-nm blue shift upon interaction with lipid, Trp^{73} apoA-V(1–146) and Trp^{128} apoA-V(1–146) underwent 11-nm shifts, consistent with their relocation to a more nonpolar environment upon lipid interaction. Compared with the other mutants, Trp^{117} appears to reside in a relatively nonpolar environment in the lipid-free conformation. At the same time, this Trp undergoes a 5-nm blue shift to 335 nm upon lipid association of the protein.

Trp Fluorescence Quenching Studies of DMPC-bound Single Trp ApoA-V Variants—To further evaluate the effect of lipid binding on solvent exposure of Trp residues in single Trp apoA-V(1–146) variants, KI and acrylamide quenching studies were conducted. In the lipid-bound state, Trp5 apoA-V(1–146) and Trp45 apoA-V(1–146) remain highly susceptible to both KI quenching and acrylamide quenching with relatively high K_{sv} constants (Table 2), whereas lipid-bound Trp^{73} apoA-V(1–146), Trp^{117} apoA-V(1–146), and Trp^{128} apoA-V(1–146) gave rise to low K_{sv} constants, suggesting protection from quenchers. Trp^{97} apoA-V(1–46) was more susceptible to acrylamide quenching than KI.

Phospholipid Vesicle Solubilization Kinetics—The data presented in Fig. 1 illustrate that apoA-V(1–146) is capable of

TABLE 2

Trp fluorescence quenching of apoA-V(1–146) variants bound to DMPC

Spectra were recorded on a Jobin Yvon FluoroMax-4 luminescence spectrometer. The average of two emission spectra were recorded from 320 to 355 nm (excitation, 295 nm) in 20 mM sodium phosphate, pH 7.4, 150 mM NaCl (slit width, 2.0 nm for the excitation and emission monochromators) at a protein concentration of 0.5 mg/ml with a DMPC:protein ratio of 5:1.

ApoA-V(1–146) single Trp variant	Predicted Trp location[a]	K_{sv}[b]	
		KI	Acrylamide
		M^{-1}	
Trp^{5}	Extreme N terminus	2.7	3.8
Trp^{45}	Polar face	2.8	3.6
Trp^{73}	Nonpolar face	1.0	2.2
Trp^{97}	Linker	1.4	4.1
Trp^{117}	Nonpolar face	1.1	2.0
Trp^{128}	Nonpolar face	1.0	2.2

[a] Based on primary sequence analysis using the Coils program (23) and Edmundson helical wheel diagrams (24).

[b] K_{sv} is the Stern-Volmer constant.

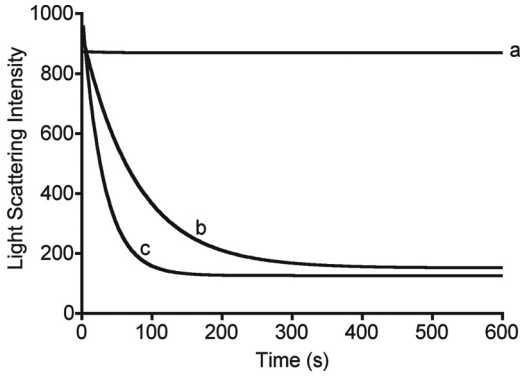

FIGURE 4. **Effect of apoA-V truncation on DMPC vesicle solubilization kinetics.** DMPC vesicles (500 μg) in 50 mM sodium citrate, pH 3.0, 150 mM NaCl, were incubated at 23 °C in the absence (*curve a*) or presence of 100 μg of full-length apoA-V (*curve b*) or apoA-V (1–146) (*curve c*). Right angle light scattering was monitored at 600 nm as a function of time.

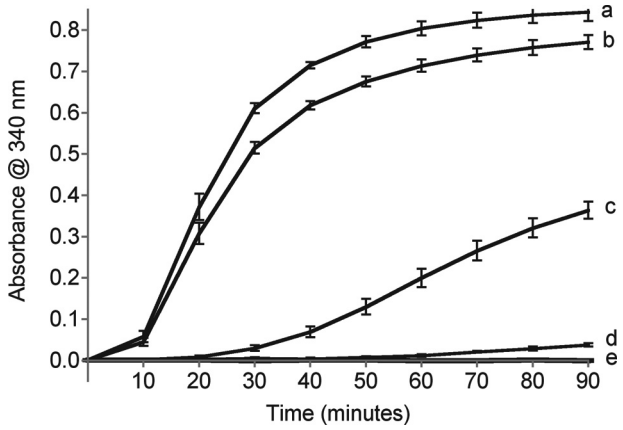

FIGURE 5. **Effect of apolipoproteins on PL-C induced aggregation of human LDL.** Human LDL (50 μg protein) was incubated at 37 °C in the absence (*curve e*) or presence (*curve a*) of PL-C (0.6 unit). Other incubations contained LDL, PL-C, and 50 μg of apoE3 NT (*curve b*), apoA-V(1–146) (*curve c*), or apoA-I (*curve d*). Sample absorbance at 340 nm was measured as a function of time. The values represent the means ± standard deviation ($n = 3$).

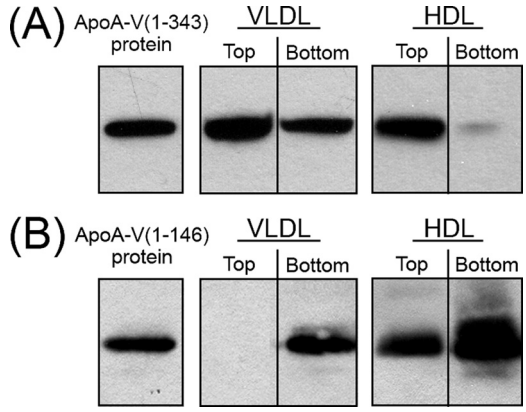

FIGURE 6. **Lipoprotein binding properties of apoA-V(1–146).** VLDL or HDL (0.1 mg/ml protein), isolated from plasma of *apoa5*$^{-/-}$ mice were incubated with 0.02 mg/ml full-length apoA-V(1–343) (*A*) or 0.01 mg/ml apoA-V(1–146) (*B*) for 1 h at 22 °C in Tris-buffered saline. Following incubation, VLDL and HDL were reisolated by density ultracentrifugation and subjected to immunoblot analysis with goat anti-human apoA-V IgG. The results shown are representative of at least three independent experiments. On the *left* of each panel is a control blot with recombinant apoA-V.

binding lipid to form reconstituted HDL. In an effort to characterize the relative lipid binding activity of this protein, kinetic analysis of apoA-V(1–146)-dependent solubilization of DMPC vesicles was measured. (Fig. 4). In control incubations lacking apolipoprotein, DMPC vesicles remain turbid with no change in solution light scattering intensity as a function of time (Fig. 4, *curve a*). Upon the addition of full-length apoA-V, a time-dependent reduction in turbidity was observed with a calculated initial rate constant (k) of $1.3 \times 10^{-2}\,s^{-1}$ (Fig. 4, *curve b*). The isolated NT domain, apoA-V(1–146), induced faster solubilization, with an initial rate constant of $3.3 \times 10^{-2}\,s^{-1}$ (Fig. 4, *curve c*).

ApoA-V(1–146) Binding to Phospholipase C Modified LDL—When human LDL is incubated with PL-C, enzymatic conversion of LDL phosphatidylcholine to diacylglycerol induces apolipoprotein association and prevents LDL particle aggregation and subsequent sample turbidity development (20). Incubation of LDL with PL-C in the absence of exogenous apolipoprotein results in rapid sample turbidity development (Fig. 5, *curve a*), whereas control incubations lacking PL-C do not develop turbidity over time (Fig. 5, *curve e*). Although incubations with recombinant human apoA-I remained clear (Fig. 5, *curve d*), incubations with apoE3 NT become turbid over time (Fig. 5, *curve b*), consistent with previous results (19). LDL incubations with PL-C in the presence of apoA-V(1–146) showed an intermediate level of protection from sample turbidity development as a function of time (Fig. 5, *curve c*).

ApoA-V(1–146) Binding to VLDL and HDL from ApoA5$^{-/-}$ *Mice*—It was previously reported that the naturally occurring truncation variant, Q139X apoA-V, does not associate with lipoproteins *in vivo* (9). To evaluate the ability of apoA-V(1–146) to associate with VLDL and HDL *in vitro*, recombinant apoA-V(1–146) was incubated with apoA-V-deficient VLDL and HDL obtained from *apoA5*$^{-/-}$ mice. Following incubation, the lipoproteins were reisolated by ultracentrifugation and analyzed by immunoblotting (Fig. 6). The data show that, whereas full-length apoA-V associates with both VLDL and HDL, apoA-V(1–146) does not associate with VLDL. Furthermore, whereas nearly all of the full-length apoA-V bound to HDL, only a fraction of apoA-V(1–146) was recovered in association with HDL.

DISCUSSION

Exchangeable apolipoproteins can transfer among lipoproteins in plasma and, in the process, likely exist in a lipid-poor

state. The helix bundle motif is postulated to facilitate this exchange by promoting apolipoprotein solubility in both polar and nonpolar environments. The size of potential lipid substrate particles is an important factor regulating apolipoprotein transfer in the circulation (25). ApoA-V is an exchangeable apolipoprotein that in humans, is found on chylomicrons, VLDL, and HDL (11). Presumably, apoA-V transfers among the different lipoprotein populations, as proposed by Nelbach *et al.* (21). The NT domain of apoA-V adopts a helix bundle conformation in the absence of lipid, and this may facilitate exchange between lipoprotein particles. In the present studies, we characterized the ability of this domain to bind to particles of various lipid compositions and sizes, including DMPC vesicles, modified LDL, and HDL and VLDL from *apoa5*$^{-/-}$ mice, in an effort to gain insight into its intrinsic lipid binding properties.

Compared with other well studied exchangeable apolipoproteins, full-length apoA-V is unique in that it is not soluble at neutral pH in a lipid-free state (6). When bound to lipid, however, apoA-V is soluble at physiological pH. This suggests that during transfer between lipoprotein particles in circulation, apoA-V may exist in a lipid-poor rather than lipid-free state. The ability of apoA-V(1–146) to form discoidal complexes with phospholipid in the size range of nascent HDL particles may be physiologically relevant because apoA-V exchange between lipoprotein particles in circulation may require transient existence in a lipid core-depleted particle.

Upon lipid interaction, it appears that apoA-V(1–146) undergoes a conformational change, as judged by an increase in α-helix secondary structure content and altered solvent exposure of reporter Trp residues. The increase in helix content upon lipid interaction is similar to that of other exchangeable apolipoproteins, such as apoA-I (26). The amphipathic helix bundle motif in the lipid-free state adopts a globular conformation wherein the hydrophobic faces of its helices orient toward the center of the bundle (27). Upon lipid association, the protein is predicted to adopt an open conformation, where the hydrophobic faces of its amphipathic helices interact directly with the lipid surface (27). Linear infrared dichroism experiments of apoA-V(1–146)·DMPC disks are consistent with a model wherein the helices orient perpendicular with respect to the DMPC bilayer fatty acyl chains. This indicates that, in the lipid-bound state, apoA-V(1–146) adopts a belt-like conformation around the perimeter of the particle, as described for other exchangeable apolipoproteins (28–33).

The lipid-induced conformational change in apoA-V(1–146) was studied using a panel of single Trp variants. Each single Trp variant reported on a specific region within apoA-V(1–146). Certain Trp residues were predicted to reside in a linker region between amphipathic helices or on the polar face of an amphipathic helix, whereas the others were predicted to reside on the nonpolar face of amphipathic helices. In keeping with these predictions, only variants with Trp predicted to reside on the hydrophobic face of amphipathic helices showed a blue shift in the wavelength of maximum fluorescence emission between alternate lipid-free and lipid-bound states. This suggests that, when presented with a suitable lipid surface, the helix bundle opens, exposing the bundle interior.

To further characterize conformational adaptations in apoA-V(1–146), the relative exposure of various regions within the NT domain were investigated as a function of lipid binding. In Trp fluorescence quenching studies, it was observed that single Trp apoA-V(1–146) variants with their Trp predicted to be on the nonpolar face of amphipathic helices gave rise to the lowest K_{sv} values, suggesting that these regions of the protein maintain close contact with the lipid surface. For example, Trp^{97} is predicted to reside in a linker region between two amphipathic helices. Consistent with this, Trp^{97} apoA-V(1–146) fluorescence emission was highly quenched by acrylamide but less so by KI. This could be due to electrostatic repulsion of KI by negatively charged residues located near Trp^{97}.

The ability of apoA-V(1–146) to initiate contact with lipid surfaces is suggested by phospholipid vesicle solubilization studies comparing truncated and full-length apoA-V. The CT domain of apoA-V has been previously shown to avidly bind lipid (7). Interestingly, despite the absence of the CT domain, apoA-V(1–146) solubilizes DMPC at a faster rate than full-length apoA-V. This suggests that N- and C-terminal domain interactions in the intact protein modulate the lipid binding properties of apoA-V. This may be similar to interactions in apoA-I. In this apolipoprotein, the CT domain initiates lipid-binding, whereas the NT helix bundle opens up to stabilize the lipid-associated state (34).

Although DMPC solubilization assays characterize apolipoprotein-induced phospholipid vesicle disruption and reorganization, PL-C-modified LDL provides a means to assess binding to spherical lipoprotein substrates. PL-C activity generates apolipoprotein-binding sites by hydrolyzing phosphatidylcholine moieties present in the surface monolayer (20). Conversion of phosphatidylcholine into diacylglycerol destabilizes the lipoprotein particle and promotes aggregation (35). Apolipoproteins protect LDL against PL-C-induced aggregation by forming a stable binding interaction with the modified particles (20). ApoA-V(1–146) binding to PL-C-treated LDL was intermediate with respect to other apolipoproteins examined. This finding is consistent with the stability properties of these apolipoproteins. At physiological pH apoA-V(1–146) is less stable than apoE3 NT (guanidine HCl denaturation midpoint of 2.0 M *versus* 2.5 M, respectively) (8, 36) yet is more stable than apoA-I (1 M guanidine HCl denaturation midpoint) (37). Thus, it appears that the intrinsic stability of helix bundle apolipoproteins in solution correlates directly with the ability to bind newly created sites on a spherical lipoprotein substrate (8).

The ability of apoA-V(1–146) to associate with physiologically relevant lipoproteins was assessed using VLDL and HDL isolated from *apoa5* knock-out mice. Importantly, apoA-V(1–146) failed to associate with VLDL and associated sparingly with HDL. This finding is intriguing in light of the report that, unlike full-length apoA-V, apoA-V(1–146) also fails to associate with intracellular lipid droplets (38). In considering the sizes of various lipid substrates, VLDL and lipid droplets are considerably larger than HDL or other lipid particles employed in this study. The data indicate that apoA-V(1–146) can associate with smaller lipid substrate particles

to a limited degree but apparently lacks the ability to interact with larger lipid particles. One explanation could be related to the tighter packing of phospholipid molecules on the surface of larger particles because of their decreased radius of curvature, as compared with smaller particles (39, 40). Tighter packing of phospholipid polar head groups enveloping a lipid core could interfere with the ability of apoA-V(1–146) to access hydrophobic surfaces and initiate binding. This aspect is obviated in the case of PL-C-modified LDL but not in the binding experiments with VLDL and HDL. In the latter case, differences in surface lipid composition and/or protein content could also influence binding of apoA-V(1–146). Regardless, it is apparent that, with natural lipoprotein substrates *in vitro*, apoA-V(1–146) binding is defective. Because this is not due to an intrinsic inability to bind lipid, it suggests that the CT of apoA-V modulates the lipid interaction properties of the NT domain.

Naturally occurring apoA-V truncations, including Q139X (9), Q148X (10), and Q97X (41), have been reported in human subjects and are associated with severe hypertriglyceridemia. The distribution of apoA-V in ultracentrifugally isolated lipoprotein classes was evaluated in several carriers of the Q139X truncation mutation and demonstrated that the truncated form of the protein does not associate with plasma lipoproteins and is found only in the lipid-poor $d >$ 1.21 g/ml fraction. Because the Q139X apoA-V mutation nomenclature includes the 23-amino acid signal peptide, the mature protein is actually 116 amino acids in length. Although apoA-V(1–146) is longer than these natural mutants, binding studies with natural lipoproteins recapitulate observations in human plasma of individuals carrying these mutant forms of apoA-V.

The present findings provide a potential explanation for the HTG observed in patients with truncated apoA-V. The lack of a CT domain alters lipid binding activity such that truncated apoA-V fails to effectively bind to circulating lipoproteins, particularly TG-rich particles. Current hypotheses suggest apoA-V interactions with heparan-sulfate proteoglycans (42, 43) and/or glycosyl phosphatidylinositol high density lipoprotein-binding protein-1 (44) indirectly enhances lipoprotein lipase activity to facilitate hydrolysis of VLDL- associated TG. The data from Nilsson *et al.* (45) indicate apoA-V also serves as a ligand for endocytic receptors of the LDL receptor family, where it is possible that apoA-V may have an important role in clearance of VLDL remnants. The putative binding site on apoA-V for lipoprotein lipase activity enhancement and cell surface molecule interactions resides within the CT domain of the protein. The absence of this binding site most likely contributes to defective hydrolysis and clearance of TG-rich lipoproteins. In any case, association of apoA-V with TG-rich lipoproteins is presumably required for manifestation of these effects. If a CT truncated apoA-V is unable to bind larger, TG-rich lipoproteins, then the resulting apoA-V-deficient particles could potentially have an increased plasma residence time, contributing to HTG. Thus, it may be that defective lipid binding arising from the lack of a CT domain precludes binding to circulating lipoproteins, thereby preventing potential TG lowering effects attributed to full-length apoA-V.

Acknowledgments—We thank Lisa Nelbach for providing mouse blood and Dr. Paul Weers for helpful discussions. We also thank Dr. Susan Marqusee for access to the circular dichroism spectrometer.

REFERENCES

1. Kamtekar, S., and Hecht, M. H. (1995) *FASEB J.* **9,** 1013–1022
2. Wilson, C., Wardell, M. R., Weisgraber, K. H., Mahley, R. W., and Agard, D. A. (1991) *Science* **252,** 1817–1822
3. Ajees, A. A., Anantharamaiah, G. M., Mishra, V. K., Hussain, M. M., and Murthy, H. M. (2006) *Proc. Natl. Acad. Sci. U.S.A.* **103,** 2126–2131
4. Breiter, D. R., Kanost, M. R., Benning, M. M., Wesenberg, G., Law, J. H., Wells, M. A., Rayment, I., and Holden, H. M. (1991) *Biochemistry* **30,** 603–608
5. Pennacchio, L. A., Olivier, M., Hubacek, J. A., Cohen, J. C., Cox, D. R., Fruchart, J. C., Krauss, R. M., and Rubin, E. M. (2001) *Science* **294,** 169–173
6. van der Vliet, H. N., Sammels, M. G., Leegwater, A. C., Levels, J. H., Reitsma, P. H., Boers, W., and Chamuleau, R. A. (2001) *J. Biol. Chem.* **276,** 44512–44520
7. Beckstead, J. A., Wong, K., Gupta, V., Wan, C. P., Cook, V. R., Weinberg, R. B., Weers, P. M., and Ryan, R. O. (2007) *J. Biol. Chem.* **282,** 15484–15489
8. Wong, K., Beckstead, J. A., Lee, D., Weers, P. M., Guigard, E., Kay, C. M., and Ryan, R. O. (2008) *Biochemistry* **47,** 8768–8774
9. Marçais, C., Verges, B., Charrière, S., Pruneta, V., Merlin, M., Billon, S., Perrot, L., Drai, J., Sassolas, A., Pennacchio, L. A., Fruchart-Najib, J., Fruchart, J. C., Durlach, V., and Moulin, P. (2005) *J. Clin. Invest.* **115,** 2862–2869
10. Priore Oliva, C., Pisciotta, L., Li Volti, G., Sambataro, M. P., Cantafora, A., Bellocchio, A., Catapano, A., Tarugi, P., Bertolini, S., and Calandra, S. (2005) *Arterioscler. Thromb. Vasc. Biol.* **25,** 411–417
11. O'Brien, P. J., Alborn, W. E., Sloan, J. H., Ulmer, M., Boodhoo, A., Knierman, M. D., Schultze, A. E., and Konrad, R. J. (2005) *Clin. Chem.* **51,** 351–359
12. Beckstead, J. A., Oda, M. N., Martin, D. D., Forte, T. M., Bielicki, J. K., Berger, T., Luty, R., Kay, C. M., and Ryan, R. O. (2003) *Biochemistry* **42,** 9416–9423
13. Fisher, C. A., Wang, J., Francis, G. A., Sykes, B. D., Kay, C. M., and Ryan, R. O. (1997) *Biochem. Cell Biol.* **75,** 45–53
14. Ryan, R. O., Forte, T. M., and Oda, M. N. (2003) *Protein Expr. Purif.* **27,** 98–103
15. Nichols, A. V., Krauss, R. M., and Musliner, T. A. (1986) *Methods Enzymol.* **128,** 417–431
16. Sreerama, N., and Woody, R. W. (1993) *Anal. Biochem.* **209,** 32–44
17. Goormaghtigh, E., Cabiaux, V., and Ruysschaert, J. M. (1990) *Eur. J. Biochem.* **193,** 409–420
18. Tallmadge, D. H., Huebner, J. S., and Borkman, R. F. (1989) *Photochem. Photobiol.* **49,** 381–386
19. Weers, P. M., Narayanaswami, V., and Ryan, R. O. (2001) *Eur. J. Biochem.* **268,** 3728–3735
20. Liu, H., Scraba, D. G., and Ryan, R. O. (1993) *FEBS Lett.* **316,** 27–33
21. Nelbach, L., Shu, X., Konrad, R. J., Ryan, R. O., and Forte, T. M. (2008) *J. Lipid Res.* **49,** 572–580
22. Lindgren, F. T., Jensen, L. C., and Hatch, F. T. (1972) in *Blood Lipids and Lipoproteins: Quantitation, Composition, and Metabolism* (Nelson, G. J., ed) pp. 181–274, Wiley-Interscience, New York
23. Lupas, A., Van Dyke, M., and Stock, J. (1991) *Science* **252,** 1162–1164
24. Schiffer, M., and Edmundson, A. B. (1967) *Biophys. J.* **7,** 121–135
25. Connelly, P. W., and Kuksis, A. (1981) *Biochim. Biophys. Acta* **666,** 80–89
26. Wald, J. H., Krul, E. S., and Jonas, A. (1990) *J. Biol. Chem.* **265,** 20037–20043
27. Segrest, J. P., Jones, M. K., De Loof, H., Brouillette, C. G., Venkatachalapa-

thi, Y. V., and Anantharamaiah, G. M. (1992) *J. Lipid Res.* **33,** 141–166
28. Raussens, V., Narayanaswami, V., Goormaghtigh, E., Ryan, R. O., and Ruysschaert, J. M. (1995) *J. Biol. Chem.* **270,** 12542–12547
29. Raussens, V., Fisher, C. A., Goormaghtigh, E., Ryan, R. O., and Ruysschaert, J. M. (1998) *J. Biol. Chem.* **273,** 25825–25830
30. Raussens, V., Drury, J., Forte, T. M., Choy, N., Goormaghtigh, E., Ruysschaert, J. M., and Narayanaswami, V. (2005) *Biochem. J.* **387,** 747–754
31. Narayanaswami, V., Maiorano, J. N., Dhanasekaran, P., Ryan, R. O., Phillips, M. C., Lund-Katz, S., and Davidson, W. S. (2004) *J. Biol. Chem.* **279,** 14273–14279
32. Martin, D. D., Budamagunta, M. S., Ryan, R. O., Voss, J. C., and Oda, M. N. (2006) *J. Biol. Chem.* **281,** 20418–20426
33. Silva, R. A., Schneeweis, L. A., Krishnan, S. C., Zhang, X., Axelsen, P. H., and Davidson, W. S. (2007) *J. Biol. Chem.* **282,** 9713–9721
34. Ji, Y., and Jonas, A. (1995) *J. Biol. Chem.* **270,** 11290–11297
35. Suits, A. G., Chait, A., Aviram, M., and Heinecke, J. W. (1989) *Proc. Natl. Acad. Sci. U.S.A.* **86,** 2713–2717
36. Wetterau, J. R., Aggerbeck, L. P., Rall, S. C., Jr., and Weisgraber, K. H. (1988) *J. Biol. Chem.* **263,** 6240–6248
37. Reijngoud, D. J., and Phillips, M. C. (1982) *Biochemistry* **21,** 2969–2976
38. Shu, X., Ryan, R. O., and Forte, T. M. (2008) *J. Lipid Res.* **49,** 1670–1676
39. Tajima, S., Yokoyama, S., and Yamamoto, A. (1983) *J. Biol. Chem.* **258,** 10073–10082
40. Wetterau, J. R., and Jonas, A. (1982) *J. Biol. Chem.* **257,** 10961–10966
41. Priore Oliva, C., Tarugi, P., Calandra, S., Pisciotta, L., Bellocchio, A., Bertolini, S., Guardamagna, O., and Schaap, F. G. (2006) *Atherosclerosis* **188,** 215–217
42. Lookene, A., Beckstead, J. A., Nilsson, S., Olivecrona, G., and Ryan, R. O. (2005) *J. Biol. Chem.* **280,** 25383–25387
43. Merkel, M., Loeffler, B., Kluger, M., Fabig, N., Geppert, G., Pennacchio, L. A., Laatsch, A., and Heeren, J. (2005) *J. Biol. Chem.* **280,** 21553–21560
44. Beigneux, A. P., Davies, B. S., Gin, P., Weinstein, M. M., Farber, E., Qiao, X., Peale, F., Bunting, S., Walzem, R. L., Wong, J. S., Blaner, W. S., Ding, Z. M., Melford, K., Wongsiriroj, N., Shu, X., de Sauvage, F., Ryan, R. O., Fong, L. G., Bensadoun, A., and Young, S. G. (2007) *Cell Metab.* **5,** 279–291
45. Nilsson, S. K., Lookene, A., Beckstead, J. A., Gliemann, J., Ryan, R. O., and Olivecrona, G. (2007) *Biochemistry* **46,** 3896–3904